

On the use of a four-cameras stereovision system to characterize large 3D deformation in elastomers

Nicolas Candau ^{a,*}, Christophe Pradille ^b, Jean-Luc Bouvard ^a, Noelle Billon ^a

^a Mines ParisTech, PSL Research University, CEMEF - Centre de Mise en Forme des Matériaux, UMR CNRS 7635, CS 10207, 06904 Sophia-Antipolis, France

^b Mat-xper, 06560 Valbonne, France

*Corresponding author: nico.candau@gmail.com

Keywords: stereo-correlation, mechanical behavior, volume change, elastomers

Abstract

The mechanical behavior and volume change of filled elastomers are studied thanks to a four-cameras stereovision system. The device allows measuring simultaneously the displacement field on two faces of the sample using 3D Digital Image Correlation (3D DIC). Subset size, step size and filter size, associated with DIC calculations, are carefully calibrated to ensure efficient analysis of the displacement fields. The smoothing parameter (i.e. filter size times step size) appears to be a discriminating criterion with an upper limit below which the strain field can be appreciably estimated. Within the appropriate choice of analysis parameters, volume changes under large deformation can be discussed. For sufficiently large deformation, volume change exhibits an upturn during stretching which could be the signature of a significant increase of void fraction. Volume change appears to be reversible during unloading phase in case maximum stretch ratio is low enough. So cavities that could have been open under tension are closed when elastic deformation is released. Conversely, for high stretching ratio, volume change exhibits a hysteresis loop-like evolution indicating that either some plastic cavities remained or closure kinetics is slower.

1. Introduction

The understanding of the mechanisms of polymer deformation has been widely improved thanks to the development of digital image correlation (DIC) methods in the 80th [1]. Recently, this approach allowed new insights on the microstructure changes induced by polymer deformation [2-5]. In some cases, DIC was coupled with complementary approaches such as X rays diffraction [2,3], in-situ scanning electron microscopy [4] or micro-computed tomography [5] to

better quantify the properties at the microscale level. Used solely, image correlation technique also provides crucial information on the strain field at the continuum mechanics macroscale level [6]. Indeed, this allows accounting for non-uniform deformation and 3D effects. An interesting improvement (compared to historical methods) consists in measuring the volume changes induced by loading making possible to address isochoric assumptions and/or damaging kinetics. This approach is particularly useful when studying the mechanisms involved in rubber materials submitted to large deformation, where cavitation, strain-induced crystallization or the concomitant effects of both take place [7]. As a matter of fact DIC is a pleasant alternative to more classical dilatometry experiments [8,9], though it is only related to the evolution of the strain field at the specimen surface.

Within the last decade, homemade [10] and commercial [11,12] image correlation analysis packages have been developed. The commercial VIC 3D® software [11] has particularly known a strong improvement and is one of the most extensively employed packages. Because of numerical calculation involved in the analysis, it offers a selection of set of parameters (subset, step, filter) to adjust for characterizing accurately the strain field. A question then arises that is to assess the sensitivity of the calculated strain field to these parameters. This was already partly studied in complex situations such as cracked propagation analysis [13], or highly non uniform deformation (such as holed tensile samples [14] or necking [15]). Nevertheless, no extensive study focused on the combined effect of such parameters on apparently homogeneous 3D strain field under large deformation, namely in elastomeric materials. Such work is however necessary to build accurately the full strain field used to access to the volume changes in the sample.

In most of the studies based on DIC or similar techniques, volume changes are estimated through the transverse isotropy assumption due to the use of 2D strain measurements. We have also to keep in mind that even a 3D displacement measurement is not pertinent enough to build a 3D strain field in the sample. It only allows accounting for the out of plane displacement of the surface of the sample. This assumption is always questionable, in particular in the case of elastomers where volume change must be investigated through the measurement of at least two faces of the tested sample.

To address volume changes using DIC in tension, several options exist with an increasing complexity. First, we can cite 2D DIC system used with an optical prism that allowed analysing two faces of the sample on one-recorded 2D-image [16, 17]. A second approach is the use of two independent cameras combining two simultaneous 2D analyses on the two faces of the sample [18]. Both these two approaches do not account properly for out of plane displacements even if telecentric lens on one hand or high depth of field system on the other hand can help a lot. Indeed, those systems require a perfect ruling of optical scene: e.g., respective orientation of lens and observed surface, focus length and aperture to rule depth of field and reduced observation zones to avoid residual aberrations of the lateral picture zones. Last solution is based on a four-cameras stereovision system (one pair of cameras system for each face) [19] that makes the

approach simpler either in terms of cameras positioning or in terms of analysis as DIC system will partly accommodate for image analysis. So, stereovision approach should ensure a proper construction of the volumic strain field provided that the image capture is correct enough (depth of field, lighting, focussing, etc.) and that the numerical analysis is performed according to the state of the art, which are of experimentalist responsibility. In spite of its strong interest, to the authors' knowledge, no study dedicated to the analysis of mechanical behaviour and volume change on elastomers submitted to high strain by using a four-cameras stereovision system was already reported in the literature.

The aim of this paper is first to illustrate such experimental methodology to characterize the mechanical behaviour and volume changes of elastomers submitted to large deformation. A special attention will be focused on the adjustments of numerical parameters involved in DIC analysis to provide a proper estimate of strain fields. Then, experimental results combining mechanical behaviour and volume change of filled elastomers during uniaxial cyclic tensile tests are discussed.

2. Materials and protocols

2.1. Materials

The materials – sample 1 and sample 2 – are two extended oil carbon black filled EPDM (Keltan 5470) obtained by sulphur vulcanization of the gum. They contain 70% in mass of Ethylene and 4.6% of Ethylidene Norbornene (ENB). They initially contain 80 phr of carbon black (80 g of fillers per 100 g of rubber) and 65 phr of paraffin oil. Within this composition, the materials are semi-crystalline with a degree of crystallinity of 2.7% (estimated from differential scanning calorimetry). Sample 1 has then been swollen in a solvent (cyclohexane) during three days and dried in vacuum during one day in order to partly remove the oil. The final oil fraction in sample 1 is found equal to 33 phr, corresponding to a decrease of weight fraction of 12% (from 27% to 15%). The main consequence is that the weight fraction of the carbon black filler is increased of 6% (from 32% to 38%). Secondly, it has been checked that the final degree of crystallinity in sample 1 after swelling and recrystallization during drying has remained down to 3%. Regarding the material processing, the gum and vulcanization recipe are sheared in an internal mixer. Sample sheets are then obtained by hot pressing at 170°C during 15 min. For tensile tests, dumbbell-shaped samples with a 15 mm gauge length (L_0), 6 mm thickness and 10 mm width, are machined.

2.2. Principle of 3D Digital image correlation (3D DIC)

3D DIC is a coupling between DIC [20] and stereovision. Stereovision makes possible to build the 3D-shape of a surface starting from two 2D plane images. DIC allows building 2D displacement field on a surface from the evolution of a random pattern. The deformation of this pattern is assumed to be joined to the deformation of the sample. Technically, two sets of images

– corresponding to two different mechanical states (i.e. reference and deformed) – are recorded with two rigidly bounded cameras between which a given angle has been set. The displacement of given points of the pattern between two pictures is determined from DIC by addressing the similarity of the grey level distributions on a subset. After determining the calibration parameters for each camera, the 3D specimen shape can be deduced from the point correspondences using triangulation. To determine the 3D displacement field, DIC is also used to determine point correspondences between the stereo pairs acquired before and after the deformation. A complete description of the 3D DIC technique can be found in the literature (e.g. Luo et al [21]). In this work, a 3D DIC method is preferred over 2D DIC for the following reasons:

- in 2D DIC, the specimen and the camera must be perfectly parallel.
- in 2D, the out of plane displacement has to be limited as it cannot be corrected. To avoid such problem, a telecentric lens could be used. In our application, this approach is not suitable due to the high deformation applied on the sample.
- the calibration lens distortions are corrected for a better accuracy of the measurements.

2.3. Experimental setup

Mechanical tests are performed with an electro-mechanic tensile test machine INSTRON 5960 at room temperature. Two loading paths are chosen. The first loading path consists in a constant nominal strain-rate unloading-unloading tests; the second one is a constant nominal strain rate loading interrupted by 5 min relaxation steps. Crosshead velocities are adjusted to promote strain rates of 0.1s^{-1} and 1s^{-1} , respectively.

The displacement fields on the front and side faces of the sample are deduced from images recorded using a four-cameras system which consists of two-pairs systems (figure 1). Four AVT cameras were used in this study. Two of them are PIKE 5 Megapixels, with a 2/3' CCD sensors (front face camera system) and the other ones are PIKE 4 Megapixels, with CCD sensors size equal to 1' (side face camera system). Both systems are respectively mounted with 25 mm and 50 mm Schneider Kreuzwach objectives. This combination of CCD sensors and objectives are chosen so that the pixels size from both systems remain close (i.e., $79\ \mu\text{m}$ and $76\ \mu\text{m}$ for front and side faces, respectively). The CCD resolution is $2452*2054$ square pixels and $2048*2048$ square pixels, respectively.

Like for a single stereovision-system, each camera pair is set up independently of the other one. Both systems are then placed in the same coordinates system using a calibration target. Sampling rate (2 Hz and 10 Hz for the strain rates 0.1s^{-1} and 1s^{-1} respectively) are chosen to ensure a low nominal strain increment between two images (0.05 and 0.1 for the strain rates 0.1s^{-1} and 1s^{-1} respectively). The exposure time of the cameras is fixed equal to 30 ms, a value three times lower than the minimum time between two image records, i.e. 100 ms (10Hz).

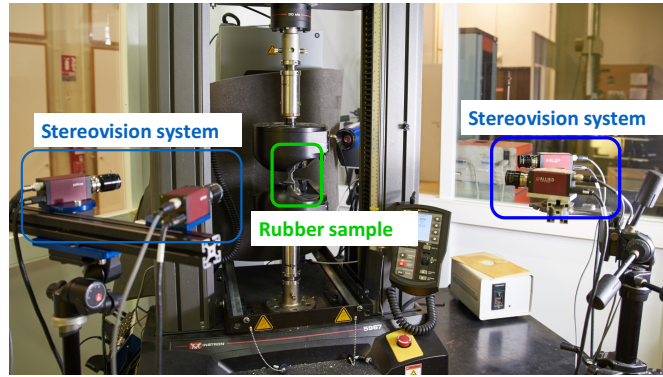


Figure 1. Experimental setup: front and side surfaces are recorder by the two independent cameras pairs system.

Front and side surfaces of the samples were coated with a white spray paint in order to generate a random speckle pattern. Large speckles are avoided as they should need large subset sizes which would reduce the spatial resolution of the analysed zone [22]. This point will be more deeply discussed in the following section. The speckles size are characterized using Image J software [23]. Prior to analysis, the camera image is thresholded and converted to a binary image. The speckles are analysed assuming a circular shape. Particles analysis then give access to the area distribution of the speckles. Figure 2b depicts typical statistical analysis of initial patterns on both the two analysed faces. The distribution is not highly broad and centred around a three pixels average size. Actually, this size is closed to the optimum mean speckle size for an accurate analysis of the strain field, which is found between 4 and 7 pixels in the study of Robert et al. [24].

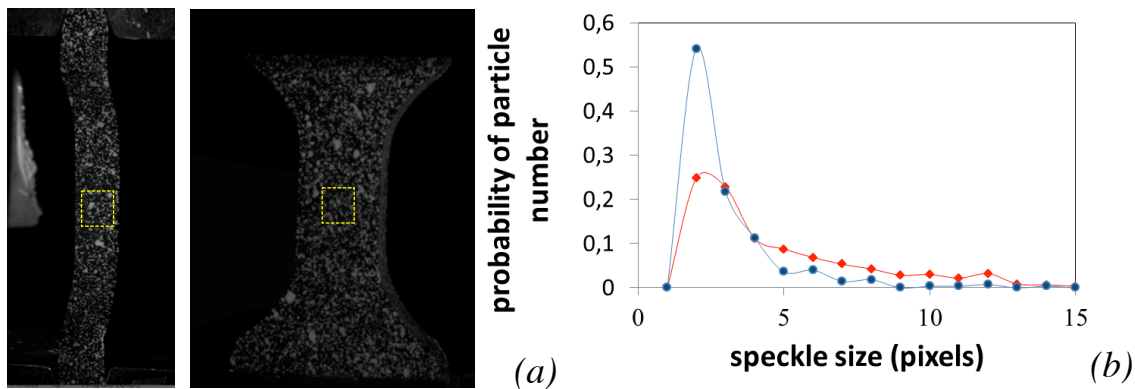


Figure 2. (a) Side and front surfaces of the specimen painted with white speckle pattern. The squares represent the analysis zones (b) Probability of the number of white speckles as a function of their size for the front face (diamond symbols) and the side face (circle symbols).

2.4. Analysis with DIC 3D

The series of images are post-processed using VIC-3D software package [11]. The first step consists in meshing a region of interest (so-called ROI) on both front and face surfaces. The meshing allows tracking the speckle pattern during the tensile test. The meshing elements are squares whose size (in pixels) is called the subset. For each subset, the strain is calculated using neighboring data points (similar to FEA models). The spacing (in pixels) of the data points are determined by the step size. To provide the best combination of spatial and displacement resolutions, the pixels of subsets are weighted by centred Gaussian functions. For the analysis, a zero normalized sum of square difference (ZNSSD) correlation criterion is used. Moreover, to reach sub-pixel resolution an interpolation of the grey level is made using quintic 8-tap splines [24].

In practice, images are generally contaminated by some noise from imaging sensors, or correlation process [1]. For reducing the noise to increase from one image to another, a non-incremental correlation has been chosen. Then, a filtering parameter (i.e. averaging) has been carefully chosen, as presented in the following section. The filter size is defined in terms of data points, which are separated by the step size. If the filter size is n , and the step size is m , the total smoothing area is $n*m$ pixels. This zone corresponds to the area where the deformation gradient is interpolated before being derived.

The 3D DIC displacement data is converted into Hencky strain (true strain) values. ϵ_1 is the true strain in the tensile direction, ϵ_2 and ϵ_3 are the transversal true strain in the directions of the sample thickness and width, respectively (figure 3a). Shear strains ϵ_{12} , ϵ_{12} and ϵ_{23} remain negligible during tensile test. However, for a proper estimate of the strain field, the strains are calculated in diagonalized coordinates space.

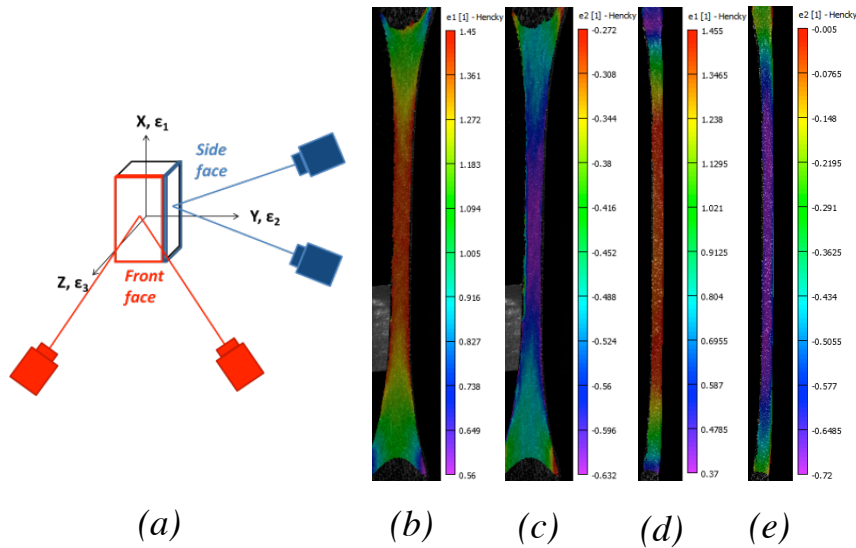


Figure 3. Schematic view of the specimen coordinates (a). Longitudinal (b) and transverse (c) strain fields in the front face of a rubber specimen stretched at the maximum extension reached during the experimental set. Longitudinal (d) and transverse (e) strain field in the side face of the same specimen.

As shown in figure 3b-e, the transverse and longitudinal strains are homogeneous in the center of the sample and significantly decrease close to the clamping zones. The strain field in both front and side faces are obtained in the central part of the sample using areas as depicted in figure 2a. Stress-strain and volume change data are extracted from such domains. The true stress is defined as the ratio between the applied force F and the surface orthogonal to the stretching axis. Then, it comes:

$$\sigma_T = \frac{F}{L_0 \exp(\varepsilon_2) e_0 \exp(\varepsilon_3)} \quad (1)$$

Where L_0 is the initial length and e_0 the initial width. The relative volume change $\Delta V/V_0$ is written as:

$$\frac{\Delta V}{V_0} = \exp(\varepsilon_1 + \varepsilon_2 + \varepsilon_3) - 1 \quad (2)$$

3. Results and discussion

3.1. Influence of the parameter analysis

A deep analysis of the volume changes requires a preliminary work focusing on the effect of the main correlation parameters (subset, step and filter) on the strain field. These parameters are analysed from pictures recorded at the maximum applied strain for the strain rate $0.1s^{-1}$. The first parameter to account for is the subset size. Figure 4 presents the values of the longitudinal strain as a function of the subset size for a range of step size varying from 1 to 25 pixels. It is known that low subset values generate an increase of the displacement uncertainty [13,25,26] as well as strain uncertainty [27]. Combined with large step sizes (20 and 25 pixels), the effect on the results is a strong underestimation of the measured strain. If the subset size decreases down to 20 pixels, the strain field analysis is even aborted.

Thus, the combination of large step and small subset appears inefficient to properly estimate the strain field. By decreasing the step size from 25 pixels to 1 pixel, the dependency of the strain on the subset size decreases. For the lowest step size values (15 pixels and below), the strain estimation does not depend on the subset size anymore. A particular case is observed for the

lowest couple of step and subset values (1, 9). True strain is underestimated compared to the series of other data obtained with the same step (step=1). This should be interpreted as an underestimation of the strain field related to the displacement uncertainty induced by a low subset size. Indeed, to be distinguished from neighboring subsets, each subset must contain a unique information (i.e. containing black and white patterns). Practically, the analysis generates holes that grow up until a complete loss of the strain field. This is consistent with the common rule of thumb which suggests that the subset must be 3 times larger than the mean speckle size [1]. Indeed, for an average speckle size measured close to 3 pixels (figure 2), the critical value of subset below which the strain field calculation is not available is around 9 pixels. Even for low step sizes, small subset should be avoided. However, to maintain a high spatial resolution of the strain field, subsets should not be too high compared to the length of the ROI (around 100 pixels for the front face and 60 pixels for the side face). In the following, the subset size will be chosen equal to 25 pixels.

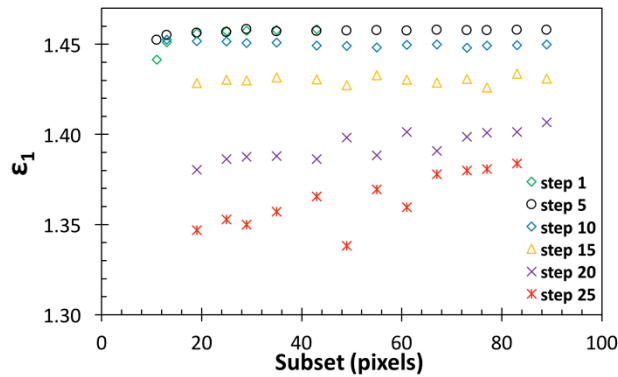


Figure 4. True strain as a function of subset size (in pixels) and different steps (in pixels) at maximum displacement for a strain rate of $0.1s^{-1}$. Filter size value is equal to 15.

The effect of the filter size is depicted in figure 5a for different step sizes. The strain increases by decreasing the filter size. This is consistent with a study of Ashrafi et al. [14], showing that the maximum principal strain measured by DIC was decreasing linearly with filter size for a more limited range of filter size values. When plotted as a function of the smoothing size, i.e. filter size*step size; all series of data points merge into a master curve (figure 5b). Thus, the combination of small step size with a large strain filter, or of large step size with a small strain filter give equivalent estimation of the strain. In a reasonable range of smoothing size, the strain reaches a threshold value. However, above a critical smoothing size around 100 pixels, the strain value dramatically decreases. This indicates that, independently of the step and filter size values, the smoothing size is the discriminating analysis parameter above which the strain cannot be significantly estimated.

As a too low filter size could lead to some noise during the calculation of the strain field [1], an intermediate value of 11 has been chosen. Concerning the step size, a minimization is crucial but its value should not be too low as the analysis time varies inversely with the square of the step

size. In the following, the analysis of the displacement of both front and side surfaces is performed with a step size of 3 pixels, and thus a smoothing size of 33 pixels. The sensibility of transversal strains ε_2 and ε_3 on the VIC analysis parameters has also been studied and leads to equivalent results than those presented in figures 4 and 5.

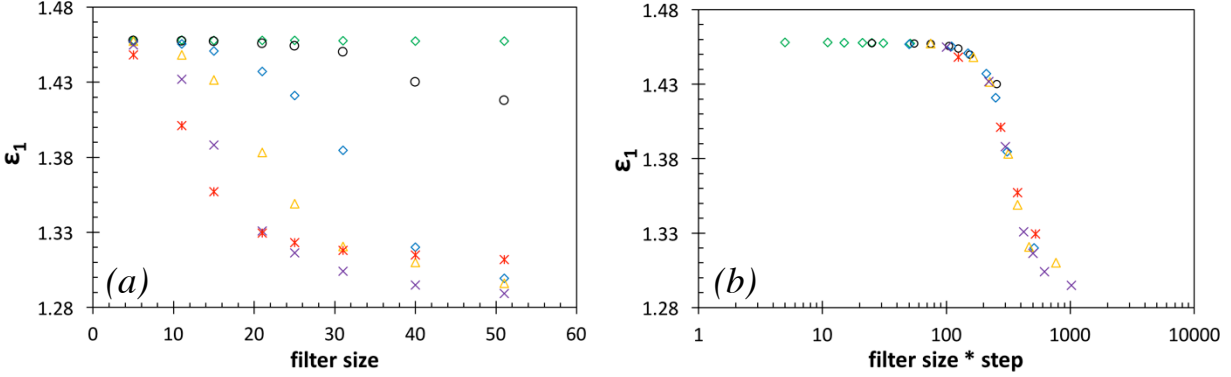


Figure 5. (a) True strain versus filter size for different steps (in pixels) at the maximum deformation of the cyclic loading at the strain rate ($0.1s^{-1}$). (b) True strain as a function of the smoothing size. The subset size is equal to 25 pixels. The symbols corresponding to the different step sizes are the same than in figure 4.

3.2. Mechanical properties and volume change at high strain

Figure 6 displays the stress-strain and the volume change curves for different camera setups: 1) four-cameras system; 2) two-camera system on the front face, 3) two-cameras system on the side face. True stress behavior and volume change are estimated from equations 1 and 2 respectively. Using the four-cameras system, we are able to measure the ratio between the transversal strains $a=\varepsilon_2/\varepsilon_3$, which is found equal to 0.9. This result is consistent with previous study from the literature [18] and is assumed to be due to an anisotropy induced by the calendaring process. Let us now consider that ε_3 is unknown, i.e. only one stereovision system for the front face is used. If we assume transverse isotropy ($\varepsilon_2=\varepsilon_3$), the true stress is overestimated, while the volume change is strongly underestimated as shown on figure 6. On the opposite, if ε_2 is missing, inverse trends are observed. We can therefore conclude that the use of transverse isotropy assumption can lead to inaccuracy when capturing the stress-strain behavior and volume change. Complete strain field measurement are thus needed.

Volume change during cyclic loading can find several reasons. They can be related to a change in the material porosity, which could be induced by void nucleation and growth. Moreover, loading could induce a phase transition (melting or crystallization under strain) and thus a change in the chains density. In contrast to EPDM with an ethylene content of 79% [28], no significant change of crystalline fraction is expected in our materials, which contain only 70% of ethylene. Moreover, the density of the ethylene crystal (1.005 g.cm^{-3}) and that of the ethylene and propylene amorphous chains (0.855 g.cm^{-3}) being relatively close, a potential change in the

crystalline fraction would have few impact on the overall density variation and consequently on volume change (a decrease of 1% of volume change roughly corresponds to an increase of 10% of the crystalline fraction). In our study, the measured volume change is thus assumed to be essentially due to the evolution of voids fraction.

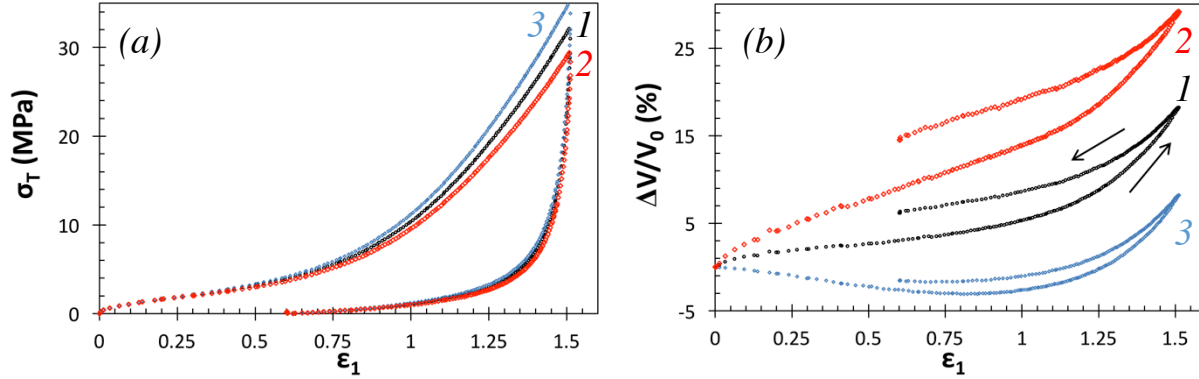


Figure 6. True stress (a) and volume change (b) versus true strain during cyclic tests at $0.1s^{-1}$ and room temperature. Volume changes are measured with 1) the four-cameras system (curve in the center), 2) with a single stereo-vision system at the front face (curve on the top) and 3) with a single stereo-vision system at the side face (curve on the bottom).

Figure 7 presents the volume change and true stress versus true strain using the four-cameras system for cyclic tests performed at $0.1s^{-1}$, at room temperature and for different maximum extensions. We can observe that volume change increases immediately after applying the deformation. This is in agreement with reference [29] while other study reported that volume change only occurs after a certain applied strain [18]. As displayed in the figure, volume changes exhibit an upturn at a strain of about 1.1. During unloading, the volume change decreases. An open hysteresis loop is observed if the maximum strain applied is sufficiently high (above the strain at the upturn), while volume change follows the same mechanical path in other case. As shown in figures 7a-b, samples exhibit a relatively high residual strain. Ex situ WAXS experiments performed on our tested samples show an increase of the diffracted intensity of the crystal planes orthogonal to the stretching direction, while the crystalline fraction measured by differential scanning calorimetry (DSC) is not modified. This is consistent with in situ SAXS from previous study [30] showing a transformation from lamellae to fibrillar transformation of the crystalline phase during the deformation of similar EPDM systems. This crystalline phase transformation as well as the viscoelastic effects strengthened by the presence of fillers should contribute to increase the residual strain as well as the mechanical hysteresis loop (figure 7b).

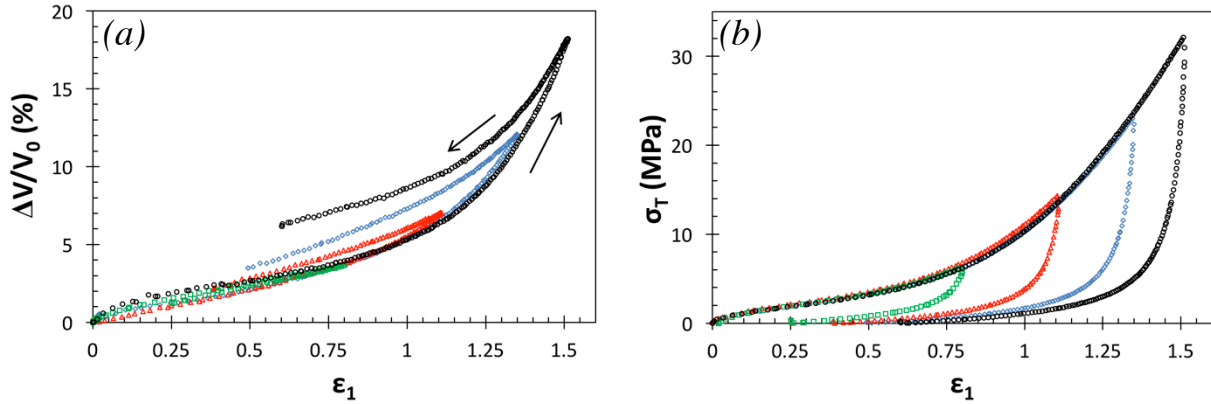


Figure 7. True stress (a) and volume change (b) versus the true strain for cyclic tests performed at $0.1s^{-1}$ and room temperature measured by the use of the 4-cameras system.

To account for the potential effect of nucleation and growth delay of cavitation during loading, relaxation steps are performed after stretching at a strain rate of $1s^{-1}$, i.e. one decade higher compared to previous tests. Figure 8 shows the evolution of volume change and true stress (in insert) as a function of the testing time. During the relaxation steps, no evolution of volume change is observed while the stress exhibits a significant relaxation likely due to strong viscoelastic effects. Thus, in the range of the experimental time, volume changes increase during loading with no delay.

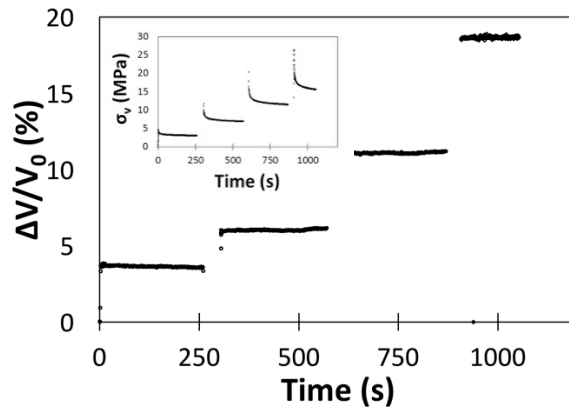


Figure 8. Volume change versus time during stretching at room temperature and with the strain rate $1s^{-1}$ interrupted by relaxation steps of five minutes.

In figure 9, mechanical properties and volume change in sample 1 are now compared to those of sample 2. The increase of oil fraction from sample 1 to sample 2 eases the chains mobility, leading to a decrease of the temperature transition of the segmental relaxation from $-30^{\circ}C$ to $-45^{\circ}C$ (see the insert in figure 9a). At room temperature (temperature of the tensile tests), the observed differences in the mechanical behavior and damage mechanisms between sample 1 and 2 should rather be mainly related to the different filler fractions (see details in the materials section). The higher content of fillers in sample 1 should mainly justify: (i) the higher elastic

modulus extracted from DMA or tensile test (figure 9a-b); and (ii) a higher strain amplification during stretching, which leads to a stronger hardening effect on the stress-strain curve (figure 9a). This hardening is concomitant with the previously discussed volume change upturn, highlighted here by comparison with sample 2 (figure 9b).

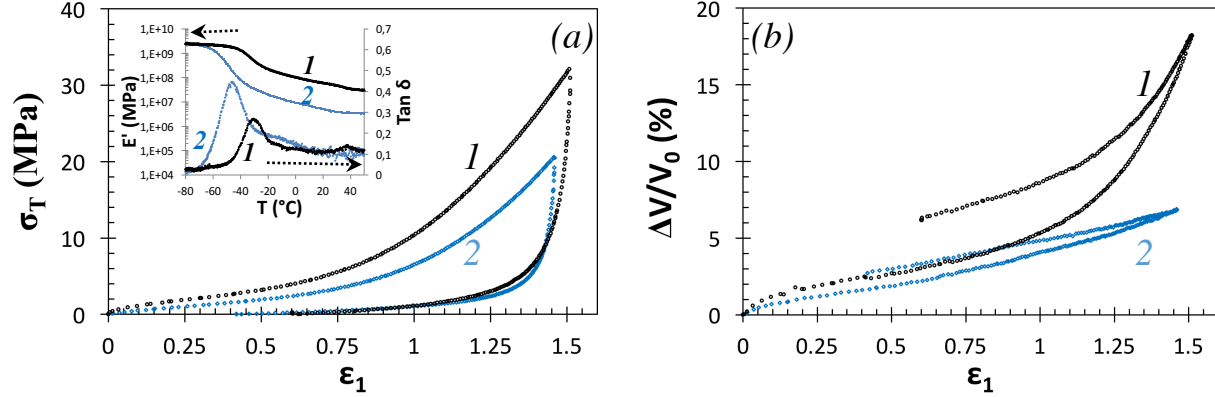


Figure 9. True stress (a) and volume change (b) versus the true strain during cyclic tests at $0.1s^{-1}$ and room temperature for sample 1 and sample 2. In insert of figure 9a are given the elastic modulus E' and the loss factor $\tan\delta$ during DMA test performed between $-80^{\circ}C$ and $50^{\circ}C$ at $1Hz$ with the strain 0.1% .

4. Conclusion

An experimental device based on a four-cameras stereovision system has been used in order to characterize the mechanical behavior and the volume change of filled elastomers. A preliminary work shows the importance of an accurate choice in the analysis parameters related to Digital Image Correlation (DIC) analysis. The combination of small step and large subset appears mandatory for a proper estimate of the strain field. The strain estimate plotted as a function of the product filter size \times step size (namely smoothing size) exhibits a master curve. It indicates that, independently of the step and filter size values, the smoothing size is a discriminating analysis parameter below which the strain can be accurately estimated. After verifying that transverse isotropy assumption may lead to inaccurate results, the complete strain field is measured. In our filled EPDM rubbers, the increase of volume changes during loading are likely due to the increase of the void fraction. In the rubber containing the larger content of fillers, volume change shows an upturn during loading. During unloading, the volume change decreases. An open hysteresis loop is observed if the maximum strain applied is sufficiently high (above the strain at the upturn), while volume change follows the same mechanical path in other case. To further analyze these mechanisms in rubber materials, the effect of crosslink density, fillers content and testing conditions (multi-loading) have been studied by using the same methodology and will be presented in subsequent papers.

5. Acknowledgements

The authors are indebted to the company SACRED for providing and processing of the rubber gum and to the laboratory GEPEA of the University of Nantes for the detailed set up of the curing procedure of rubber materials. This work was performed in the framework of the project ECOTHER supported by BPIFrance.

6. References

- [1] M. Sutton, J-J Orteu, H Schreier. Image Correlation for Shape, Motion and Deformation Measurements: basic concepts, theory and applications. Springer Science & Business Media, 2009.
- [2] J. Engqvist, M. Wallin, S. A. Hall, M. Ristinmaa, T. S. Plivelic. Measurement of multi-scale deformation of polycarbonate using X-ray scattering with in-situ loading and digital image correlation. *Polymer* 2016; 82:190.
- [3] H. Zhang, A. K. Scholz, J. De Crevoisier, F. Vion-loisel, G. Besnard, A. Hexemer, H. R. Brown, E. J. Kramer, C. Creton. Nanocavitation in Carbon Black Filled Styrene – Butadiene Rubber under Tension Detected by Real Time Small Angle X-ray Scattering. *Macromolecules* 2012; 45(3):1529.
- [4] J. M. Teixeira Pinto, F. Touchard, S. Castagnet, C. Nadot-Martin, D. Mellier. DIC Strain Measurements at the Micro-Scale in a Semi-Crystalline Polymer. *Experimental Mechanics* 2013; 53(8):1311.
- [5] M. F. Arif, N. Saintier, F. Meraghni, J. Fitoussi, G. Rober. Multiscale fatigue damage characterization in short glass fiber reinforced polyamide-66. *Composites Part B: Engineering* 2014; 61:55.
- [6] R. Moulart, S. Avril, F. Pierron. Identification of the through-thickness rigidities of a thick laminated composite tube. *Composites Part A: Applied Science and Manufacturing* 2004; 32(7):326.
- [7] J. Le Cam, E. Toussaint. Volume Variation in Stretched Natural Rubber : Competition between Cavitation and Stress-Induced Crystallization. *Macromolecules* 2008; 41(20):7579.
- [8] R. W. Penn, “Volume Changes Accompanying the Extension of Rubber. *Transactions of The Society of Rheology* 1970; 14(4):509.
- [9] J-M. Chenal, C. Gauthier, L. Chazeau, L. Guy, Y. Bomal. Parameters governing strain induced crystallization in filled natural rubber. *Polymer* 2007; 48(23):6893.
- [10] L. Chevalier, S. Calloch, F. Hild, Y. Marco. Digital image correlation used to analyze the multiaxial behavior of rubber-like materials. arXiv preprint physics/0511148 2005.
- [11] S. Vic-3D (2007) ®Software. Correlated Solutions Incorporated, Columbia.

- [12] Aramis 2D software (2008), GOM Optical Measuring Techniques. <http://www.gom.com/EN/index.html>.
- [13] I. Eshraghi, M. R. Yadegari Dehnavi, N. Soltani. Effect of subset parameters selection on the estimation of mode-I stress intensity factor in a cracked PMMA specimen using digital image correlation. *Polymer Testing* 2014; 37:193.
- [14] M. Ashrafi, M. E. Tuttle. High Strain Gradient Measurements in Notched Laminated Composite Panels by Digital Image Correlation. *Composite, Hybrid, and Multifunctional Materials*, Volume 4. Springer International Publishing, 2015; 75-81.
- [15] E. Parsons, M. C. Boyce, D. M. Parks. An experimental investigation of the large-strain tensile behavior of neat and rubber-toughened polycarbonate. *Polymer* 2004; 45(8):2665.
- [16] E. Parsons, M. C. Boyce, D. M. Parks, M. Weinberg. Three-dimensional large-strain tensile deformation of neat and calcium carbonate-filled high-density polyethylene. *Polymer* 2005; 46(7): 2257.
- [17] N. Temimi-Maaref, A. Burr, N. Billon. Damaging processes in a commercial polypropylene compound. *Experimental and modelling. Polymer Science, Series A* 2008; 50(5): 558.
- [18] J. de Crevoisier, G. Besnard, Y. Merckel, H. Zhang, F. Vion-Loisel, J. Caillard, D. Berghezan, C. Creton, J. Diani, M. Brieu, F. Hild, S. Roux. Volume changes in a filled elastomer studied via digital image correlation. *Polymer Testing* 2012; 31(5):663.
- [19] M. Sutton, J. H. Yan, V. Tiwari, H. W. Schreier, J. J. Orteu. The effect of out-of-plane motion on 2D and 3D digital image correlation measurements. *Optics and Lasers in Engineering* 2008, 46(10):746.
- [20] M. Sutton, W. Wolters, W. Peters, S. McNeill S. Determination of displacements using an improved digital correlation method. *Image and Vision Computing* 1983; 1:133.
- [21] P. Luo, Y. Chao, M. Sutton, W. Peters. Accurate measurement of threedimensional deformations in deformable and rigid bodies using computer vision. *Experimental Mechanics* 1993; 30(2):123.
- [22] M. Bornert, F. Brémand, P. Doumalin, J.-C. Dupré, M. Fazzini, M. Grédiac, F. Hild, S. Mistou, J. Molimard, J.-J. Orteu, L. Robert, Y. Surrel, P. Vacher, B. Wattrisse. Assessment of Digital Image Correlation Measurement Errors: Methodology and Results. *Experimental Mechanics* 2008; 49(3):353.
- [23] U. Rasband WS (1997–2011) ImageJ, US National Institutes of Health, Bethesda, Maryland.

- [24] L. Robert, F. Nazaret, T. Cutard, J.-J. Orteu. Use of 3-D Digital Image Correlation to Characterize the Mechanical Behavior of a Fiber Reinforced Refractory Castable. *Experimental Mechanics* 2007; 47(6):761.
- [25] H. Schreier, J. Braasch, M. Sutton. Systematic errors in digital image correlation caused by intensity interpolation. *Opt. Eng* 2000; 39(11):2915.
- [26] V. P. Rajan, M. N. Rossol, F. W. Zok. Optimization of Digital Image Correlation for High-Resolution Strain Mapping of Ceramic Composites. *Experimental Mechanics* 2012; 52(9):1407.
- [27] S. Bergonnier, F. Hild, J.-B. Rieunier, and S. Roux. Strain heterogeneities and local anisotropy in crimped glass wool. *Journal of Materials Science* 2005; 40(22):5949.
- [28] L. Liu, B. S. Hsiao, B. X. Fu, S. Ran, S. Toki, B. Chu, A. H. Tsou, P. K. Agarwal. Structure Changes during Uniaxial Deformation of Ethylene-Based. *Macromolecules* 2003; 36(6):1920.
- [29] J. Ramier, L. Chazeau, C. Gauthier, L. Stelandre, L. Guy, E. Peuvrel-Disdier. In situ SALS and volume variation measurements during deformation of treated silica filled SBR. *Journal of Materials Science* 2007; 42(19):8130.
- [30] E. Planes, L. Chazeau, J. Vigier, JM. Chenal, T Stuhldreier. Crystalline Microstructure and Mechanical Properties of Crosslinked EPDM Aged Under Gamma Irradiation. *Journal of Polymer Science: Part B: Polymer Physics* 2010; 48:97.